ENHANCED RESOLUTION OF FLUORESCENCE ANISOTROPY DECAYS BY SIMULTANEOUS ANALYSIS OF PROGRESSIVELY QUENCHED SAMPLES

Applications to Anisotropic Rotations and to Protein Dynamics

JOSEPH R. LAKOWICZ, HENRYK CHEREK, IGNACY GRYCZYNSKI, NANDA JOSHI, AND MICHAEL L. JOHNSON
University of Maryland at Baltimore, School of Medicine, Department of Biological Chemistry, Baltimore, Maryland 21201

ABSTRACT   Enhanced resolution of rapid and complex anisotropy decays was obtained by measurement and analysis of data from progressively quenched samples. Collisional quenching by acrylamide was used to vary the mean decay time of indole or of the tryptophan fluorescence from melittin. Anisotropy decays were obtained from the frequency-response of the polarized emission at frequencies from 4 to 2,000 MHz. Quenching increases the fraction of the total emission, which occurs on the subnanosecond timescale, and thereby provides increased information on picosecond rotational motions or local motions in proteins. For monoexponential subnanosecond anisotropy decays, enhanced resolution is obtained by measurement of the most highly quenched samples. For complex anisotropy decays, such as those due to both local motions and overall protein rotational diffusion, superior resolution is obtained by simultaneous analysis of data from quenched and unquenched samples. We demonstrate that measurement of quenched samples greatly reduces the uncertainty of the 50-ps correlation time of indole in water at 20°C, and allows resolution of the anisotropic rotation of indole with correlation times of 140 and 720 ps. The method was applied to melittin in the monomeric and tetrameric forms. With increased quenching, the anisotropy data showed decreasing contributions from overall protein rotation and increased contribution from picosecond tryptophan motions. The tryptophan residues in both the monomeric and the tetrameric forms of melittin displayed substantial local motions with correlation times near 0.16 and 0.06 ns, respectively. The amplitude of the local motion is twofold less in the tetramer. These highly resolved anisotropy decays should be valuable for comparison with molecular dynamics simulations of melittin.

INTRODUCTION

Fluorescence anisotropy decays provide information on the size, shape, flexibility, and interactions of biological macromolecules (1–4). For a rigid spherical molecule the anisotropy decays as a single exponential. Measurement of a single rotational correlation time is moderately easy with either time-resolved or steady-state measurements. However, few if any macromolecules are spherical and rigid. Multiexponential anisotropy decays are expected for asymmetric proteins (5, 6) and asymmetric molecules (7, 8), and still more complex anisotropy decays are expected for

hindered probes in membranes or for macromolecules with segmental flexibility (9, 10). Resolution of these complex decays is complicated by the inherently low signal-to-noise ratio of anisotropy data, which is a difference between the individual polarized components. The individual components can be threefold to severalfold larger than the magnitude of the difference. Of course, the noise in the difference is determined by the noise in the individual measurements, which is typically given by the square root of the number of photons.

One approach for increased anisotropy resolution is the use of more advanced instrumentation (11–13). For time-domain measurements the introduction of pulsed laser sources provides increased intensity, increased pulse rates, and decreased data acquisition times. Also important is the dramatic reduction in the instrument response functions. For the older flash lamp and standard photomultiplier tube (PMT) systems the instrument response functions are typically near 2 ns. For picosecond pulses from a dye laser and a microchannel plate PMT, the instrument response can be reduced to 100 ps. Additionally, the introduction of

signal averaging with streak cameras has increased the signal-to-noise ratio and hence improved the resolution. For instance, correlation times near 150 ps have been measured for ethidium bromide in water, and times near 50 ps have been estimated for tryptophan derivatives in water (14, 15).

The available resolution has also been enhanced by the introduction of frequency-domain fluorometers (16, 17). These instruments allow measurement of the frequency-response of the emission, which is used to recover the time-domain parameters. Originally, these instruments had upper frequency limits of 200 MHz. However, recent improvements increased the upper limit to 2,000 MHz (18). The frequency-domain instruments provide excellent resolution of complex and rapid anisotropy decays. Correlation times as short as 15 ps have been measured (19).

Here we described a simple method to further improve the resolution of anisotropy decays measured in either the time or the frequency-domain. Our experimental data are only in the frequency-domain. We use collisional quenching to vary the decay time of the sample. For instance, consider a protein with a lifetime (τ) of 4 ns, and assume the fluorescent residue is held rigidly by the protein, which itself has a rotational correlation time (θ) of 4 ns. The information on the anisotropy decay is contained in the difference between the parallel ($I_\parallel$) and perpendicular ($I_\perp$) components of the emission (Fig. 1, *left*). For the 4-ns correlation time (*dashed lines*), the difference persists throughout the duration of the emission, and all the emitted photons aid in recovering the anisotropy decay. Now suppose the correlation time is 400 ps (*solid lines*). Then, the polarized components are essentially equal after 1 ns, and the photons detected after this time do not aid in recovering the anisotropy decay. However, the emitted photons all contributed to the emission and to the acquisition time. Because the acquisition times must be finite, and systematic errors or instrumental drifts are always present, it is difficult to collect data adequate to determine the picosecond correlation time.

Now consider the effect of decreasing the decay time to a subnanosecond value of 0.4 ns by quenching (Fig. 1, *right*). Few of the observed photons are held for nanoseconds, so resolution of the global rotation will be diminished. However, an increasing fraction of the emitted light contains information on the picosecond motion, as this is the only process that is significant on the subnanosecond timescale. Hence, information on the faster process is increased by measurement of the quenched samples.

For rapid monoexponential anisotropy decays analysis of data from the most quenched sample is adequate. However, we desired improved resolution of the entire anisotropy decay. This was accomplished by simultaneous analysis of data from the unquenched and several quenched samples. The data from the unquenched sample contribute most to the determination of the longer correlation times, and the data from the quenched sample contribute to resolution of the faster events. The improved resolution is illustrated by measurements of the anisotropic rotations of indole, and by the resolution of overall rotation and local tryptophan motions in the monomeric and tetrameric forms of melittin.

THEORY

Suppose a sample is excited with a brief pulse of vertically polarized light (Fig. 1). If the fundamental anisotropy is greater than zero ($r_0 > 0$), the polarized excitation results in a larger population of molecules whose emission is alligned parallel to the excitation. After excitation, the initial difference between the parallel ($I_\parallel^Q(t)$) and perpendicular ($I_\perp^Q(t)$) components of the emission decays due to both rotational motions of the fluorophore and to decay of the total emission ($I_T^Q(t)$). The individual polarized components decay as

$$I_\parallel^Q(t) = \tfrac{1}{3}I_T^Q(t)[1 + 2r(t)] \qquad (1)$$

$$I_\perp^Q(t) = \tfrac{1}{3}I_T^Q(t)[1 - r(t)], \qquad (2)$$

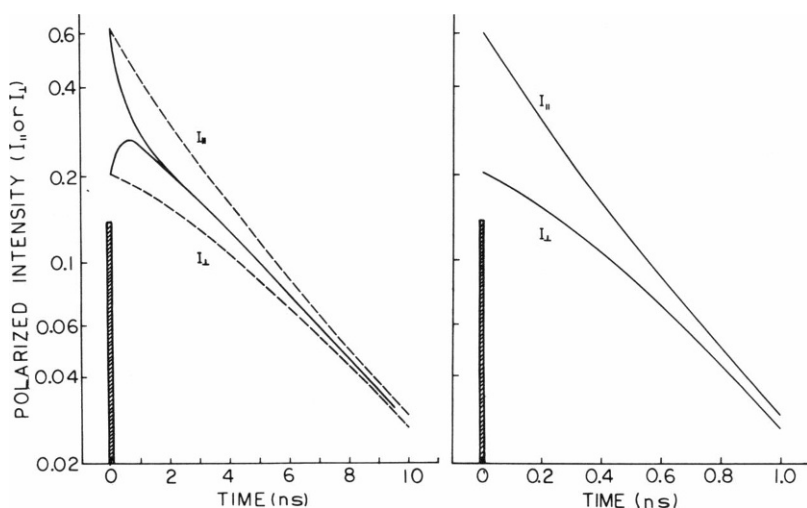FIGURE 1 Simulated anisotropy decays for unquenched and quenched decays. (*Left*) Unquenched decay with τ = 4 ns and θ = 4 (*dashed lines*), or 0.4 ns (*solid lines*). (*Right*) Quenched decay with τ = 0.4 ns and θ = 0.4 ns. r_0 is 0.4 for both decays.

where the total emission is

$$I_T^Q(t) = I_\parallel^Q(t) + 2I_\perp^Q(t). \tag{3}$$

The superscript Q indicates the quencher concentration. Information about the rotational motions is contained in the anisotropy decay law, which can be described as a sum of exponentials

$$r(t) = \sum_i r_0 g_i e^{-t/\Theta_i}. \tag{4}$$

It is of interest to determine $r(t)$ with the highest possible resolution because the correlation times (Θ_i) and the associated amplitudes ($r_0 g_i$) are determined by the size, shape, and flexibility of the molecule. For asymmetric molecules rotating freely in solution, the values of Θ_i are functions of the rotational diffusion coefficients about the principle axes. The amplitudes depend on the orientation of the absorption and emission dipoles relative to these axes (5–8). For proteins the apparent correlation times are determined by the rates of rotational diffusion and by segmental motions of the fluorophore relative to the protein.

Our approach to improving resolution is to vary the intensity decay $I_T^Q(t)$ by collisional quenching. We assume that collisional quenching does not alter the anisotropy decay, which seems to be reasonable as many quenchers do not appear to interact with the fluorophores or proteins. We note that if the quencher altered the anisotropy decay, this effect would be revealed by an inability to simultaneously fit the data measured at several quencher concentrations to a single anisotropy decay law.

We measure the anisotropy decays in the frequency domain. The measured quantities are the phase angle difference between the parallel and perpendicular components of the emission ($\Delta_\omega^Q = \phi_\perp - \phi_\parallel$) and the ratio of the modulated components of the polarized emission ($\Lambda_\omega^Q = m_\parallel/m_\perp$), each measured over a range of modulation frequencies (ω). The anisotropy decay parameters are obtained by the best nonlinear least squares fit to the data using calculated (c) values of Δ_ω^Q and Λ_ω^Q (20, 21). The calculated values are obtained using

$$\Delta_{c\omega}^Q = \arctan\left(\frac{D_\parallel^Q N_\perp^Q - N_\parallel^Q D_\perp^Q}{N_\parallel^Q N_\perp^Q + D_\parallel^Q D_\perp^Q}\right) \tag{5}$$

$$\Lambda_{c\omega}^Q = \left[\frac{(N_\parallel^Q)^2 + (D_\parallel^Q)^2}{(N_\perp^Q)^2 + (D_\perp^Q)^2}\right]^{1/2} \tag{6}$$

where

$$N_i^Q = \int_0^\infty I_i^Q(t) \sin \omega t \, dt \tag{7}$$

$$D_i^Q = \int_0^\infty I_i^Q(t) \cos \omega t \, dt. \tag{8}$$

The goodness-of-fit is estimated from the value of reduced chi-squared

$$\chi_R^2 = \frac{1}{\nu}\sum_{\omega,Q}\left(\frac{\Delta_\omega^Q - \Delta_{c\omega}^Q}{\sigma_\Delta}\right)^2 + \frac{1}{\nu}\sum_{\omega,Q}\left(\frac{\Lambda_\omega^Q - \Lambda_{c\omega}^Q}{\sigma_\Lambda}\right)^2, \tag{9}$$

where ν is the number of degrees of freedom (number of data points minus the number of floating parameters) and σ_Δ and σ_Λ are the uncertainties in the phase angle and modulation ratio, respectively. If the data are obtained for several quencher concentrations, the data can be analyzed simultaneously to obtain the anisotropy decay (Eq. 4). Alternatively, data at a single quencher concentration can be used to determine $r(t)$. At each quencher concentration the intensity decay ($I_T^Q(t)$) must be determined, as it is needed to calculate the values of $\Delta_{\omega c}^Q$ and $\Lambda_{\omega c}^Q$.

We now prefer a modified form for the modulation ratio Λ_ω. We define (19, 21) the frequency-dependent or modulated anisotropy as

$$r_\omega = \frac{\Lambda_\omega - 1}{\Lambda_\omega + 2}. \tag{10}$$

The values of r_ω are comparable to those of the steady-state anisotropy (r) and the fundamental anisotropy (r_0). At low modulation frequencies, r_ω is nearly equal to r. At high modulation frequencies, r_ω approaches r_0.

The anisotropy data were always fit to expressions like Eq. 4, but two variations were used. In some cases the total anisotropy was considered to be a unknown parameter, so the variable terms in Eq. 4 were the values for Θ_i and the $r_0 g_i$. In other cases the fundamental anisotropy was assumed to be known, so the variable terms were the Θ_i and g_i, with $\Sigma\,g_i = 1.0$. If r_0 is accurately known, this additional constraint improves the resolution of the anisotropy decay (21, 22). This is especially true for rapid anisotropy decays, for which limited time resolution results in a decrease in the apparent value of r_0.

MATERIALS AND METHODS

Frequency-domain data were obtained on a recently constructed instrument with a upper frequency limit of 2 GHz (18). The improved bandwidth was obtained by two modifications of our previous instrument (17). The continuous laser source was replaced with a cavity dumped dye laser, 5-ps pulses at 3.7931 MHz. This source provides harmonic content at each interger multiple of the pulse rate to many gigahertz. Detection of the high frequency components was accomplished with a microchannel plate PMT with external cross-correlation. The data are transferred to a dedicated Minc 11/23 computer for analysis. For all analyses the estimated uncertainties were 0.2° in the phase angle and 0.005 in the modulation (23).

Indole was recrystallized from petroleum ether, and acrylamide was from Aldrich Chemical Co. (Milwaukee, WI), gold label lot HMO2820KL. Melittin, from Serva Fine Biochemicals, Inc. (Garden City Park, NY; cat. No. 51560), is claimed to be pure by high performance liquid chromatography (HPLC) and free of N-formylmelittin. A second sample of synthetic melittin was provided by Dr. Frank Prendergast (Mayo Foundation, Rochester, MN). Most of the data were obtained using the more plentiful sample from Serva Fine Biochemicals, Inc., and the results confirmed using the synthetic melittin. Gel electrophoresis of the melittin (both Serva and the synthetic sample) indicated a single dominant band that accounted for ~98% of the staining material

(12% gel). HPLC analysis of both melittin samples indicated purities in excess of 95%.

Indole and melittin were excited at 300 nm, and the emission was observed through a WG320 filter for the frequency-domain measurements. Emission spectra were taken of all the quenched and unquenched samples and were found to agree with the expected spectra. Melittin displayed the expected blue shift in the presence of 2 M NaCl (24). Acrylamide quenching constants for indole in water and for melittin were in agreement with the expected values (25, 26; Eftink, M. R., personal communication). The emission spectra did not display any obvious spectral shifts in the presence of quenching. For steady-state and intensity decay measurements, magic angle polarizer orientation was used (4). Unless indicated otherwise all measurements were in 10 mM Tris, pH 7.0, 20°C. The values of r_0 were determined at 300-nm excitation -65°C for indole in propylene glycol (0.296) and in 67% propylene glycol/buffer for melittin (0.305). Acrylamide did not have a substantial effect on the viscosity of water or propylene glycol. In water, 2 M acrylamide increased the viscosity by no more than 5%. In propylene glycol 2 M acrylamide decreased the viscosity by $\sim$7%. These changes are not significant for the present analysis.

RESULTS

Anisotropic Rotation of Indole in Propylene Glycol

Indole in propylene glycol was chosen to provide a decay of anisotropy, which was both rapid and complex. Indole is a disk-like molecule, and it seemed probable that it would display two correlation times as the result of more rapid in-plane rotations and less rapid out-of-plane rotations. The temperature (20°C) was selected to result in a mean correlation time near 0.5 ns. The resolution of a subnanosecond anisotropy decay with two correlation times must be regarded as a challenging task.

The frequency-response data for the intensity decays of indole are shown in Fig 2. As the concentration of acrylamide is increased the frequency response is shifted towards higher frequencies, which indicates a more rapid intensity decay. In the absence of acrylamide the intensity decay is essentially a single exponential. This is seen by the good match between the data (*solid circles*) and the calculated response for a single decay time (Fig. 2), and the low value of χ_R^2 (Table I). The value of χ_R^2 did not improve significantly for a two decay time analysis. In the presence of acrylamide quenching the intensity decays become more complex than a single exponential. This is seen by the inability to account for the data with a single decay time, as seen by the calculated curve (*solid line*) and the systematic deviations (Fig. 2, *lower panel, open circles*). We found the intensity decay could be adequately fit using a two decay time model (Fig. 2, *dashed line;* Table I). The decays become increasingly heterogeneous with increased quenching, as indicated by the increasing values of χ_R^2 for the one decay time fits. We believe that the increasing heterogeneity is due to the transient terms in the Smoluchowski diffusion equations (27, 28). In fact, the data at quencher concentrations below 0.5 M in propylene glycol can be explained by an intensity decay of the form $I(t) = \exp(-t/\tau - 2b\sqrt{t})$. However, a theoretically correct form for
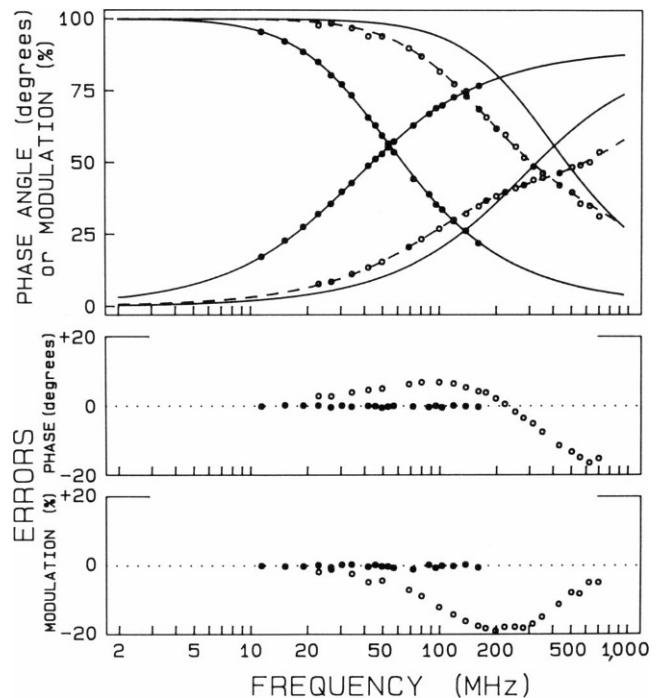

FIGURE 2 Frequency-response for the intensity decay of indole in propylene glycol at 20°C. Phase and modulation data are shown at 0 and 1.5 M acrylamide. *Dashed lines,* the best two decay time fits to the 1.5 M data; *solid lines,* the best one decay time fits. The lower panel shows the deviations between the data and the best single decay time fits for 0 (*solid circles*) and 1.5 M (*open circles*) acrylamide. For the one decay time fits the values of χ_R^2 are 0.9, and 1,115 at 0 and 1.5 M acrylamide, respectively.

the intensity decay is not necessary for the anisotropy analysis. The only necessity is that the intensity decay be represented numerically in Eqs. 7 and 8. The double exponential decays in Table I are adequate for this purpose.

To avoid confusion it should be noted that all values of χ_R^2 are calculated using the same value for the uncertainties in the phase and modulation data (0.2° and 0.005, respectively). As the concentration of acrylamide is increased the value of χ_R^2 increases for the two decay time fits. The values of χ_R^2 did not increase significantly for a three decay time analysis. The modest twofold elevation in χ_R^2 is probably due to an increased noise level for measurements on the more quenched samples. Because of the fixed values of the uncertainties, only the relative values of χ_R^2 are useful in selecting the appropriate fit to the data (23).

Frequency-domain anisotropy data at various acrylamide concentrations are shown in Fig. 3. Several features of the data are worthy of noting. As the quencher concentration is increased the data were measured to higher frequencies. This is because the extent of demodulation is less at each frequency in the quenched samples (Fig. 2). At present it is the demodulation or "bandwidth" of the samples, which determines the upper frequency limit, and not the bandwidth of the instrument. In the presence of

TABLE I

INTENSITY DECAY PARAMETERS FOR INDOLE
IN PROPYLENE GLYCOL AT VARIOUS
ACRYLAMIDE CONCENTRATIONS, 20°C

[Acrylamide]	τ_i	α_i	f_i	χ_R^2
M	*ns*			
0	4.35	1.0	1.0	0.9*
	3.51	0.13	0.10	
	4.67	0.87	0.90	0.9‡
0.3	2.46	1.0	1.0	57.0
	0.88	0.25	0.09	
	2.85	0.75	0.91	1.3
0.5	1.77	1.0	1.0	129.0
	0.80	0.43	0.20	
	2.38	0.57	0.80	1.8
1.0	0.92	1.0	1.0	362.0
	0.33	0.58	0.24	
	1.44	0.42	0.76	2.2
1.5	0.59	1.0	1.0	1,115.0
	0.18	0.74	0.29	
	1.24	0.26	0.71	3.2
2.0	0.44	1.0	1.0	2,125.0
	0.12	0.81	0.31	
	1.20	0.19	0.69	2.1

*Single exponential fit.
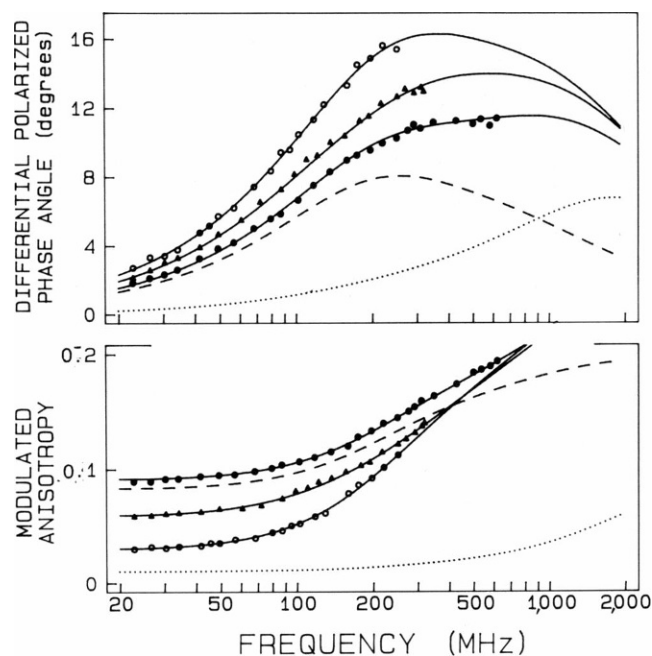‡Double exponential fit.

FIGURE 3 Frequency-domain anisotropy data for indole in propylene glycol at 20°C. Data are shown for 0 (*open circles*), 0.5 (*triangles*), and 1.0 M (*solid circles*) acrylamide. *Dashed lines*, Differential phase angles and modulated anisotropies expected for a single correlation time of 0.7 ns and $r_0 g_2 = 0.2$, using the intensity decay law of indole with 1 M acrylamide (Table I); *dotted lines*, data expected for a correlation time of 0.1 ns and $r_0 g_1 = 0.1$, and the 1 M decay law.

quenching the differential phase angles of indole show increased evidence of the multiple correlation times. This is particularly noticeable for 1 M acrylamide (Fig. 3, *solid circles*), for which the phase angles become constant with frequency, rather than the usual Lorentzian distribution for a single correlation time. The increased phase angles at higher frequencies are due to the shorter correlation time. This fact is illustrated by the dashed line, which shows expected values for a single correlation time of 0.7 ns. The dotted line shows expected values for a 0.1-ns correlation time. The modulated anisotropies also show a marked dependence on quenching. The values at low frequencies (<50 MHz) represent the elevation in the steady-state anisotropy due to quenching. The high frequency values tend towards the value of $r_0 = 0.296$, but this value is not reached because of the 0.12-ns component in the decay.

The data for each acrylamide concentration can be analyzed individually to recover an anisotropy decay, or analyzed simultaneously (Table II). As the decay time is decreased by quenching, the anisotropy decay is recovered with greater resolution. For instance, with r_0 as a floating parameter, it was just possible to determine two correlation times for the unquenched sample. While the results for the two correlation time fits are correct, the decrease in χ_R^2 is a modest 39% relative to the single correlation time fit. Also, the uncertainties in the correlation times and amplitudes are large, and the final values from the analysis were somewhat sensitive to the starting values. For the single correlation time fit the apparent value of r_0 (0.23–0.20) is smaller than the expected value. When data from the quenched samples are analyzed, both correlation times are more easily recovered, as is the expected value of r_0. For instance, a one correlation time fit to the data for 1 M acrylamide yields an unacceptable value of $\chi_R^2 = 4.4$. Use of a two correlation time model yields $\chi_R^2 = 0.68$, the expected value for r_0, correlation times of 0.12 and 0.66 ns, and much smaller uncertainties in the correlation times and the amplitudes. For this series of samples one notices that the ability to discriminate between one and two correlation times increases progressively as the lifetime is decreased (Table II).

The resolution can be further enhanced by simultaneous analysis of the data for all five acrylamide concentrations. The ratio of χ_R^2 for the one and two correlation time fits is similar for the single file fit and for the five file simultaneous fit. The ratio is more significant for the five-file fit because of the larger number of degrees of freedom (29). Of course, if the lifetime becomes too short the longer correlation time will eventually be determined with less precision. The advantage of simultaneous analysis of data for several quencher concentrations is that both longer and shorter correlation times can be recovered for the same sample, as will be shown below for melittin.

If the value of the fundamental anisotropy (r_0) is known, then it is advantageous to use this value in the analysis (Table II, *lower half*). With the known value of r_0 for

TABLE II
ANISOTROPY DECAY PARAMETERS FOR INDOLE IN PROPYLENE GLYCOL 20°C

[Acrylamide]	θ_i	$r_0 g_i$	χ^2_R
M	ns		
r_0 = floating parameter			
0	0.61	0.232‡	1.06
	0.10 (0.23)*	0.130 (0.13)§	
	0.70 (0.54)	0.194 (0.03)§	0.76
0.5	0.57	0.239	2.07
	0.02	0.510	
	0.67	0.202	0.95
1.0	0.51	0.254	4.44
	0.12 (0.03)	0.103 (0.005)	
	0.66 (0.03)	0.193 (0.011)	0.68
1.5	0.51	0.261	6.9
	0.19	0.133	
	0.82	0.157	0.83
2.0	0.49	0.267	7.57
	0.16	0.123	
	0.76	0.171	0.87
0–2.0	0.51	0.260	8.80
	0.14 (0.004)	0.120 (0.003)	
	0.72 (0.11)	0.179 (0.003)	1.21
r_0 = 0.296 = fixed parameter			
0	0.46	0.296 = C	24.1
	0.12	0.104	
	0.70	0.192	0.75
0.5	0.42	0.296 = C	36.3
	0.13	0.111	
	0.70	0.185	1.02
1.0	0.38	0.296 = C	41.1
	0.12	0.103	
	0.66	0.193	0.67
1.5	0.38	0.296 = C	41.1
	0.15	0.125	
	0.77	0.171	0.84
2.0	0.36	0.296 = C	95.2
	0.15	0.120	
	0.75	0.176	0.86
0–2.0	0.39	0.296 = C	46.1
	0.15	0.122	
	0.73	0.174	1.21

*The numbers in parentheses indicate the uncertainties in the values estimated from the nonlinear least squares fit, assuming the parameters are not correlated (29).
‡Single correlation time fit.
§Two correlation time fit.

indole it was possible to recover the two correlation times in the absence of quenching, with a 30-fold decrease in χ^2_R. Examination of the one and two correlation time fits shows greater χ^2_R ratios at each quencher concentration and for the global fit. Use of the r_0 value becomes more important as the correlation times become shorter, and falls within the time resolution of the measurements.

The uncertainty limits of the correlation times can be determined by examination of the χ^2_R surface. The parameter in question is held constant at a value different from the χ^2_R minimum, and the remaining parameters are varied to again yield the minimum possible value of χ^2_R. For indole we held one correlation time constant, and allowed χ^2_R to reach a new minimum with the second correlation time and the two amplitudes ($r_0 g_i$) as floating parameters. This is a powerful test of the resolution because it accounts for correlation between the parameters.

Some χ^2_R surfaces for indole are shown in Fig. 4. In the absence of quenching there is little sensitivity of χ^2_R to the two correlation times with r_0 as a floating parameter. This is seen from the weak dependence of χ^2_R on the values of the correlation times (Fig. 4, *left, dashed line*). Better resolution of the two correlation times is found if the value of r_0 is fixed (Fig. 4, *right, dashed line*). In contrast, the χ^2_R values are highly sensitive to the correlation times when the indole is quenched with 1.5 M acrylamide (*dotted lines*). Still greater resolution was found for simultaneous analysis of all five data sets (*solid lines*), and it should be recalled that smaller elevations in χ^2_R are significant due to the fivefold higher number of data points and degrees-of-freedom. These results indicate that complex anisotropy decays can be recovered with greater confidence by simultaneous analysis of quenched and unquenched samples.

Resolution of Picosecond Correlation Times

It is of interest to measure picosecond correlation times for comparison of experimental data with molecular dynamics calculations (30–34). Hence we examined the effect of quenching on our ability to recover the anisotropy decay of indole in water at 20°C. Once again, the intensity decays become more complex in the presence of quenching. This is evident from the increase in χ^2_R for the single decay time fits (Table III). The double decay time model provided a good fit to the data, or seen by the low values of χ^2_R, and from the good match of the calculated and experimental
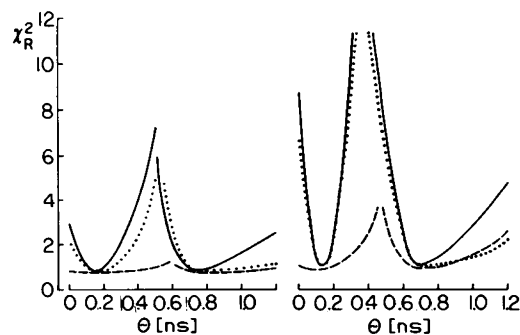

FIGURE 4 Dependence of χ^2_R on the correlation times of indole. (*Left*) χ^2_R surfaces with r_0 as a floating parameter; (*right*) the surface with r_0 as a fixed parameter, equal to 0.296. In each panel the χ^2_R surface is shown for the unquenched sample (*dashed lines*), the sample with 1.5 M acrylamide (*dotted lines*), and for simultaneous analysis of the five samples, 0–2 M acrylamide (*solid lines*).

TABLE III
INTENSITY DECAYS OF INDOLE IN WATER IN THE PRESENCE OF ACRYLAMIDE

[Acrylamide]	τ_i	α_i	f_i	χ_R^2
M	*ns*			
0	4.50	1.0	1.0	2.2
0.025	2.42	1.0	1.0	7.3
	1.14	0.13	0.06	
	2.58	0.87	0.94	1.7
0.1	0.94	1.0	1.0	134.0
	0.32	0.35	0.13	
	1.18	0.65	0.87	2.0
0.3	0.49	1.0	1.0	216.0
	0.08	0.51	0.16	
	0.45	0.49	0.84	2.6

TABLE IV
ANISOTROPY DECAY PARAMETERS FOR INDOLE IN AQUEOUS BUFFER AT 20°C

[Acrylamide]	θ	r_0	χ_R^2
M	*ps*		
r_0 = floating parameter			
0	66	0.208	1.1
0.025	74	0.181	0.40
0.10	54	0.281	1.9
0.30	50	0.322	2.3
0–0.3	48	0.322	3.2
	46	0.316	
	90	0.01	3.3*
r_0 = 0.296 = fixed			
0	46	0.296 = C	1.1
0.025	44	0.296 = C	0.5
0.10	51	0.296 = C	2.0
0.30	56	0.296 = C	3.5
0–0.3	53	0.296 = C	3.8

*Two correlation time fit.

frequency responses (not shown). Acrylamide quenching reduced the decay time ~10-fold (Table III), and consequently the frequency-domain anisotropy data could be measured to 2 GHz (Fig. 5).

Analysis of the anisotropy data indicates a substantial increase in resolution of the 50-ps correlation time by measurement of the quenched samples. In the absence of quenching, with r_0 as a floating parameter, the correct correlation time was recovered (Table IV). However, 30% of the anisotropy was not recovered as the apparent value of r_0 was only 0.208. It should also be noticed that the value of χ_R^2 is only weakly dependent on the correlation time, especially with r_0 as a floating parameter (Fig. 6, *left, dashed line*). Recovery of the correct correlation time in

this case must be the result of the high signal-to-noise ratio of the measurements and an absence of significant systematic errors.

As the lifetime of indole is decreased by quenching it become possible to recover the total anisotropy even for this 50-ps correlation time. For instance, the values of r_0 recovered from the analysis were 0.28 at 0.1 M and 0.32 at 0.3 M acrylamide (Table IV), which agrees with the measured value of 0.296 in propylene glycol at −65°C. The improved resolution is especially apparent from the χ_R^2 surfaces (Fig. 6). The values of χ_R^2 are considerably more sensitive to the correlation time for the quenched samples, even for changes as small as 5 ps. Once again, the value of using the known value of r_0 is seen by the greater sensitivity of χ_R^2 when r_0 is fixed (Fig. 6, *right*). Surprisingly, the sensitivity of χ_R^2 to the 50-ps correlation time is somewhat less for the simultaneous analysis (*solid lines*) than for analysis of the most quenched sample (*dotted lines*). Of
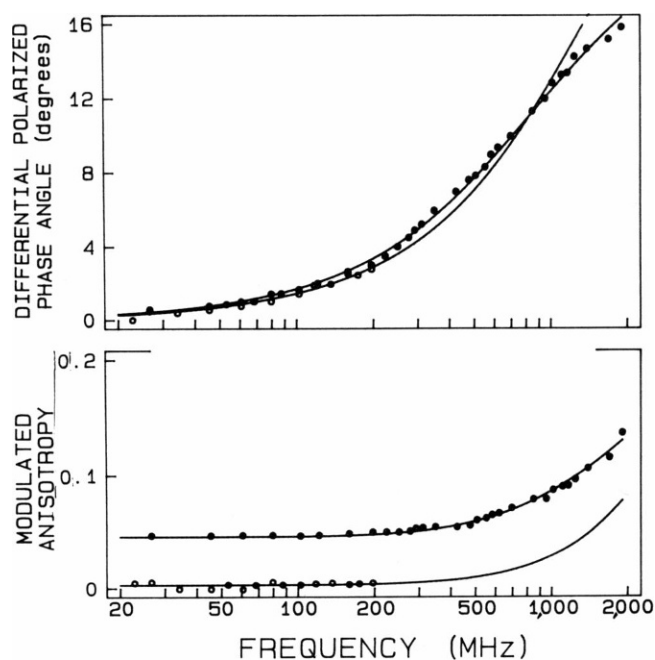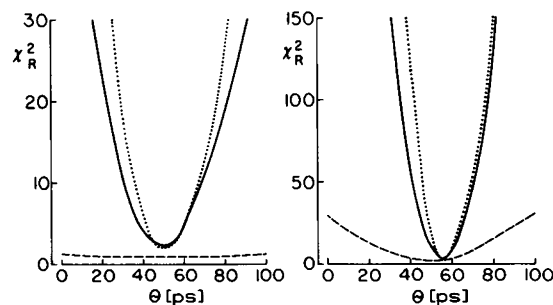

FIGURE 5 Frequency-domain anisotropy data for indole in aqueous buffer at 20°C. Data are shown for acrylamide concentrations of 0 (*open circles*) and 0.3 M (*solid circles*).

FIGURE 6 Dependence of χ_R^2 on the correlation time of indole in water at 20°C. (*Left*) χ_R^2 surfaces with r_0 as a floating parameter; (*right*) χ_R^2 surfaces with r_0 = 0.296 as a fixed parameter. In each panel the χ_R^2 surface is shown for the unquenched sample (*dashed lines*), the sample with 0.3 M acrylamide (*dotted lines*), and for three samples (0, 0.1, and 0.3 M acrylamide, *solid lines*) (Table III).

TABLE V
INTENSITY DECAYS OF MELITTIN IN THE PRESENCE OF ACRYLAMIDE

[Acrylamide]	τ_i	α_i	f_i	χ_R^2	[Acrylamide]	τ_i	α_i	f_i	χ_R^2
M	*ns*				*M*	*ns*			
0 M NaCl, monomer					2 M NaCl, tetramer				
0	0.88	0.36	0.12		0	0.74	0.44	0.17	
	3.72	0.64	0.88	2.8*		2.95	0.56	0.83	10.6
	0.24	0.32	0.03			0.23	0.32	0.04	
	2.12	0.33	0.30			1.99	0.58	0.67	
	4.22	0.36	0.66	1.2‡		4.95	0.10	0.29	0.9
0.2	0.23	0.55	0.18		0.2	0.34	0.51	0.18	
	1.26	0.45	0.82	6.1		1.56	0.49	0.82	4.0
	0.12	0.51	0.10			0.16	0.43	0.08	
	0.91	0.41	0.62			1.05	0.42	0.54	
	2.01	0.08	0.28	1.5		2.14	0.15	0.38	0.9
0.5	0.12	0.76	0.34		0.5	0.19	0.63	0.23	
	0.78	0.24	0.66	22.9		1.08	0.37	0.77	4.7
	0.05	0.73	0.19			0.11	0.59	0.15	
	0.50	0.25	0.64			0.78	0.35	0.61	
	2.03	0.02	0.17	2.0		1.76	0.06	0.24	0.9
1.0	0.08	0.83	0.37		1.0	0.15	0.69	0.28	
	0.66	0.17	0.63	39.0		0.87	0.31	0.72	18.2
	0.04	0.79	0.25			0.07	0.64	0.15	
	0.41	0.20	0.58			0.55	0.32	0.61	
	1.90	0.01	0.18	2.7		1.71	0.04	0.24	1.2
1.5	0.08	0.88	0.47		1.5	0.08	0.80	0.31	
	0.63	0.12	0.53	45.0		0.66	0.20	0.69	21.5
	0.03	0.81	0.28			0.04	0.78	0.22	
	0.31	0.18	0.54			0.45	0.20	0.58	
	1.77	0.01	0.18	1.9		1.55	0.02	0.70	1.9
2.0	0.06	0.92	0.54		2.0	0.08	0.86	0.42	
	0.62	0.08	0.46	40.4		0.71	0.14	0.58	38.6
	0.02	0.88	0.32			0.04	0.77	0.23	
	0.26	0.11	0.48			0.29	0.20	0.46	
	1.39	0.01	0.20	2.7		1.22	0.03	0.31	3.2

*Double exponential fit.
‡Three exponential fit.

course, this is the result of using data from the unquenched samples, which are less sensitive to the correlation time. However, this small decrease in sensitivity is not significant because of the large number of data points used in the simultaneous analysis.

Anisotropy Decay of Melittin

Melittin is an amphipathic peptide containing 26 amino acid residues, with a single tryptophan residue at position 19. In solution melittin can exist as either a monomer (low salt) or a tetramer (high salt). The monomeric form of melittin is thought to be largely a random coil (24, 35) with a high degree of segmental mobility (22). In the tetrameric state the monomeric units are mostly α-helical, with the four tryptophan residues in a low density hydrophobic pocket. We used the quenching method to obtain highly resolved anisotropy decays of melittin. Since the x-ray structure is known (36), we believe these highly resolved anisotropy decays could be compared with molecular dynamics calculations on this same protein.

We measured the intensity and anisotropy decays of melittin at six acrylamide concentrations from 0 to 2 M. Typical intensity decay data are shown in Fig. 7. The presence of acrylamide shifted the frequency-response towards higher frequencies. Even at the highest acrylamide concentrations the signal-to-noise ratio was adequate at all measurable frequencies. The emission spectra were characteristic of melittin at all acrylamide concentrations (not shown). The background fluorescence did not exceed 1% at acrylamide concentrations up to 1 M. Above 1 M acrylamide the background fluorescence did not exceed 4% of the signal due to the melittin. It was necessary to use three decay times to characterize the intensity decays of melittin, both in the presence and absence of quencher (Fig. 7, *solid lines*). This is seen by the average 11-fold decrease in χ_R^2 found for comparison of the two and three decay time fits (Table V). It should be mentioned that these data contain
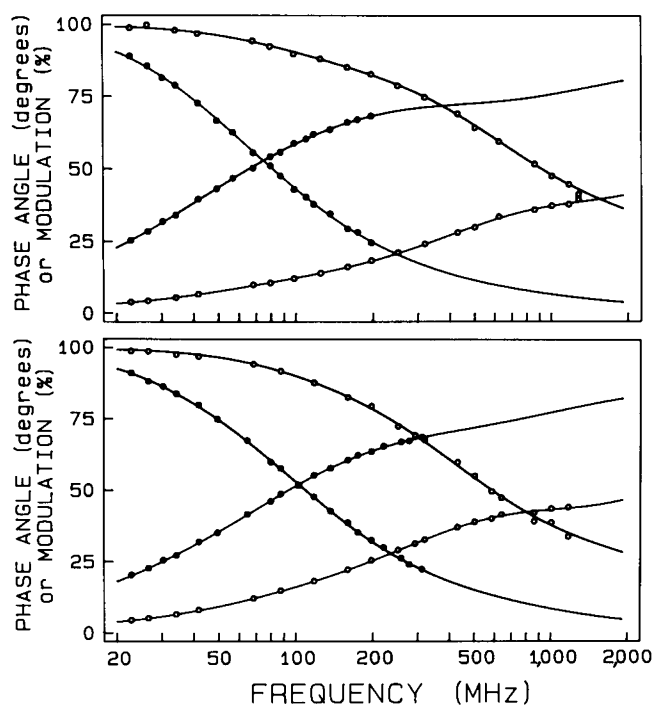
FIGURE 7   Intensity decay data for mellitin in the absence (*solid circles*) and presence (*open circles*) of 2 M acrylamide. (*Top*) Melittin monomer; (*bottom*) melittin tetramer. The solid lines show the best fit to the data using three decay times (Table V).

information on the diffusion rates of acrylamide within the tetramer, but calculation of these rates is outside the scope of this paper.

The frequency-domain anisotropy data for the melittin tetramer nicely illustrate the effect of quenching on the information content of the measurements (Fig. 8). As the quencher concentration is increased the contribution of overall protein rotation is decreased, and the contribution of the torsional motions is increased. Overall protein rotation is responsible for the maximum in the phase angle near 100 MHz, as can be seen from the simulated curve for a 3.4-ns correlation time (*dashed lines*). The 60-ps motion is responsible for the increasing phase angles above 500 MHz, which can be seen from the simulated curve for 60 ps (*dotted lines*). Upon quenching, the contribution of overall protein rotation is diminished, while that of the segmental motion is increased. It seems evident that the combined data will provide increased resolution of the total anisotropy data, above that obtainable from any single set of data.

Similar data were obtained for the monomeric melittin (Fig. 9). In this case the differential phase angles do not show a dominant component due to overall protein rotation, but rather show increased dispersion of the frequency response. Of course, this is because the monomeric state is disordered and highly flexible. The dispersed frequency response is the result of both the shorter overall correlation time for the monomer, and the possibility that three
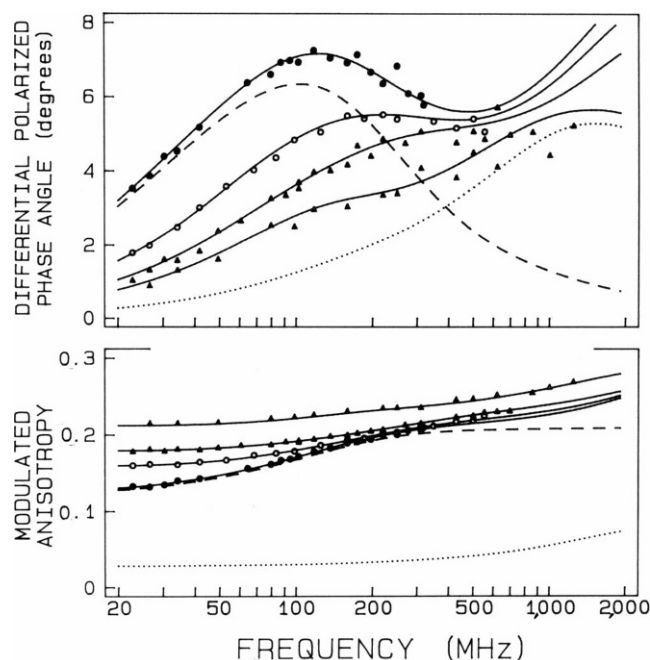

FIGURE 8   Frequency-domain anisotropy data for melittin tetramer, 2 M NaCl, 20°C. Data are shown for acrylamide concentrations of 0 (*solid circles*), 0.2 M (*open circles*), 0.5 M (*solid triangles*), and 2.0 M (*open triangles*) acrylamide. *Solid lines,* best simultaneous fit to the data (0–2 M) using two correlation times; *dashed lines,* simulated values for a single correlation time of 3.4 ns, $r_0 g_i = 0.21$, and the intensity decay for melittin tetramer with no acrylamide (Table V); *dotted line,* simulated values for a correlation time of 60 ps, $r_0 g_i = 0.12$, and the intensity decay for mellitin tetramer with 2.0 M acrylamide (Table V).
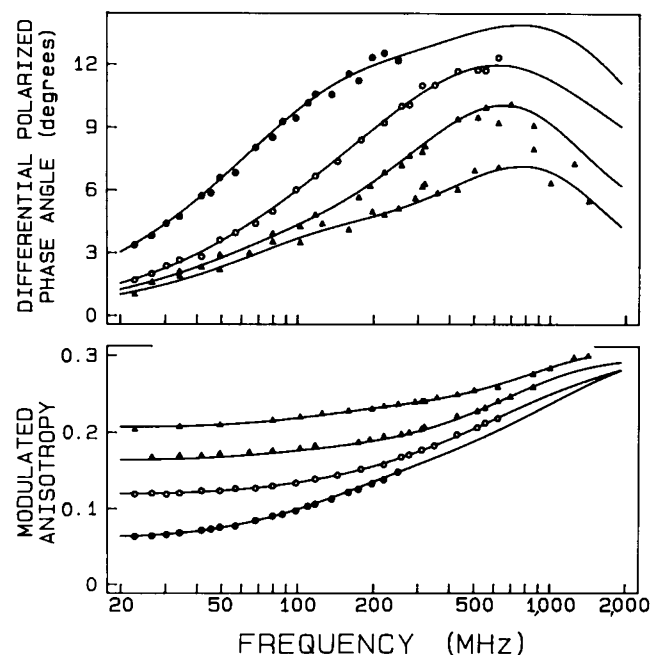

FIGURE 9   Frequency-domain anisotropy data for melittin monomer, 0 M NaCl, 20°C. Data are shown for 0 (*solid circles*), 0.2 (*open circles*), 0.5 (*solid triangles*), and 2.0 M (*open triangles*) acrylamide. The solid lines show the best simultaneous fit to the data (0–2 M) using two correlation times.

LAKOWICZ ET AL.   *Molecular Dynamics of Melittin*

correlation times are needed to describe the anisotropy decay. The value of measuring quenched samples for flexible molecules is evident from the increasing phase angles at the higher frequencies, which are due to the rapid segmental motions. Without quenching these higher frequency components would not be measurable due to demodulation of the emission.

Resolution of the melittin anisotropy decays is increased by analysis of the data from the quenched samples. This is seen by the increasing ratio of χ_R^2 for the one and two correlation time fits as the concentration of acrylamide is increased (Tables VI and VII). It should also be noticed that essentially the same anisotropy decay is recovered at each concentration of acrylamide, which indicates that the intensity and the anisotropy decays are not coupled, and that acrylamide does not alter the anisotropy decay. The χ_R^2 surfaces illustrate the effects of quenching on the resolution. The sensitivity of χ_R^2 to the 3.4-ns correlation time of the monomer is decreased by quenching (Fig. 10). This is because quenching decreases the contribution of this correlation time to the data (Fig. 8). In contrast, quenching enhances the sensitivity of χ_R^2 to the 60-ps component. For overall resolution it is best to simultaneously analyze the multiple data sets, as both long and short correlation times are determined with greater accuracy (Fig. 10, *solid lines*). It should be noted that the data are not consistent with a correlation time significantly shorter than 60 ps, as seen by the increase in χ_R^2.

The anisotropy decay data were analyzed in a number of ways. The fits and parameters we believe are best supported by the data are indicated in Tables VI and VII. These time-resolved decays are plotted in Fig. 11. Since the value of χ_R^2 for the simultaneous analyses are not much larger than that of the individual analyses, it is not likely that the anisotropy decay is altered by presence of the quencher. The anisotropy decay of melittin tetramer is due to both a 60-ps component, which accounts for 36% of the anisotropy decay, and a 3.4-ns component due to overall rotational diffusion accounting for 68% of the anisotropy decay. The anisotropy decay of the monomer shows a higher percentage (58%) due to a fast process (160 ps), and the remaining anisotropy decays with a correlation time near 1.7 ns. Although not shown, we occasionally found slightly improved fits for the monomer using three correlation times. The third correlation time was often near 300 ps. If such results were obtained consistently the intermediate correlation time would be assigned to motions of peptide chain, which includes the tryptophan residue. With the present level of resolution we prefer to accept the two correlation time fit (0.16 and 1.73 ns) as best describing the anisotropy decay of monomeric melittin. The larger apparent short correlation time for the monomer (160 ps) as compared with the tetramer (60 ps) is probably due to contributions from slower motions of the peptide chain. To ensure reliability of the anisotropy decays we also examined a sample of synthetic melittin, generously provided by

TABLE VI
ANISOTROPY DECAYS OF MELITTIN, MONOMER, No NaCl

[Acrylamide]	θ_i	$r_0 g_i$*	χ_R^2
M	*ns*		
0	1.09	0.203	14.6[‡]
	0.24	0.173	
	1.94	0.118	0.8[§]
0.2	0.71	0.251	46.3
	0.17	0.188	
	1.78	0.132	0.7
0.5	0.61	0.276	33.2
	0.16	0.182	
	1.93	0.138	1.2
1.0	0.49	0.292	34.9
	0.15	0.194	
	1.90	0.133	2.1
1.5	0.47	0.298	23.9
	0.14	0.191	
	1.81	0.138	1.9
2.0	0.43	0.305	19.5
	0.14	0.181	
	1.48	0.146	3.3
Global analysis			
0–2 M	0.55	0.287	70.3
	0.45	0.305 = C	93.9
	2 ps = C	1.076	
	0.77	0.240	31.9
Fig. 11[‖]	0.16	0.187	
	1.73	0.136	2.4
	2 ps = C	0.024	
	0.16	0.186	
	1.74	0.135	2.4[¶]
	−0.001	−0.032	
	0.16	0.186	
	1.74	0.135	2.4**

*Unless indicated otherwise the total anisotropy was a floating parameter in the analysis. The term "= C" indicates the parameter was held constant at the indicated value.
[‡]Single correlation time fit.
[§]Two correlation time fit.
[‖]Fits and parameters that are best supported by the data.
[¶]Three correlation time fit.
**Global analysis (0–2 M acrylamide) with three floating correlation times and amplitudes.

Dr. F. Prendergast. These results, summarized in Table VIII, are essentially equivalent to those found for our sample of melittin.

A number of theoretical studies have predicted correlation times of 2 ps or shorter for aromatic residues in proteins (30). For example, a rapid component in the anisotropy decay of bovine pancreatic trypsin inhibitor, due to torsional motions of the tyrosine residues, was calculated to be complete in <2 ps (31–33). Similarly, molecular dynamic calculations on lysozyme indicated that

TABLE VII
ANISOTROPY DECAYS OF MELITTIN TETRAMER, 2 M NaCl

[Acrylamide]	θ_i	$r_0 g_i$*	χ_R^2
M	ns		
0	2.95	0.220	9.8
	0.09	0.094	
	3.48	0.205	0.96
0.2	2.61	0.228	20.1
	0.11	0.078	
	3.57	0.204	1.1
0.5	2.31	0.236	21.5
	0.06	0.109	
	3.41	0.207	0.91
1.0	2.05	0.244	19.5
	0.12	0.080	
	3.67	0.204	0.82
1.5	1.59	0.259	32.0
	0.08	0.096	
	3.60	0.208	1.6
2.0	1.43	0.265	40.6
	0.07	0.107	
	3.63	0.209	2.3
Global analysis			
M			
0–2	2.12	0.244	62.9
	0.88	0.305 = C	537.6
	2 ps = C	1.507	
	2.96	0.219	5.3
Fig. 11[‡]	0.06	0.118	
	3.40	0.208	2.0
	2 ps = C	0.810	
	0.17	0.047	
	3.59	0.203	1.7
	2 ps = C	−0.024[§]	
	0.06	0.120	
	3.40	0.208	1.7

*Unless indicated otherwise the total anisotropy was a floating parameter in the analysis. The term "= C" indicates the parameter was fixed at the indicated value.
[‡]Fits and parameters that are best supported by the data.
[§]$r_0 = 0.305$ was a fixed parameter.

the anisotropy of some of its tryptophan residues decays on this timescale, but it should be noted that some of the individual tryptophan anisotropies continue to decay to 15 ps (34). Hence, we questioned whether our data on melittin were consistent with a 2-ps component in the anisotropy decay. However, we stress that our experimental data are for melittin, and not the proteins used in the previously mentioned simulations (30–34).

We attempted to fit the data using a fixed correlation time of 2 ps. The data for either the monomer or for the tetramer were not consistent with a significant 2-ps motion. These attempts to find a 2-ps motion were initially done with a three correlation time model. In the case of the
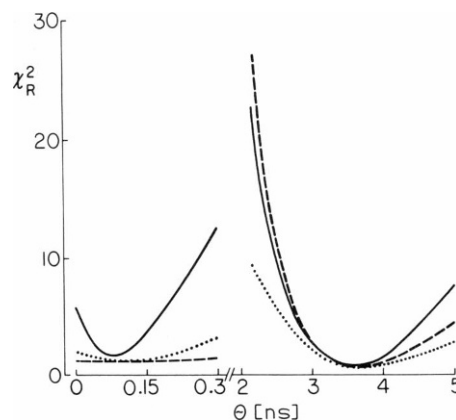

FIGURE 10 Dependence of χ_R^2 on the correlation times for melittin tetramer. These surfaces are shown for 0 (*dashed lines*) and 0.5 M acrylamide (*dotted lines*) and for a simultaneous analysis with data from 0–2 M acrylamide (*solid lines*).

monomer, inclusion of a fixed 2-ps correlation time resulted in a small amplitude for this motion (Table VI). In the case of the tetramer a fixed 2-ps correlation time resulted in either an unreasonable amplitude for the motion or in a small amplitude (Table VII). If the data are fit to two correlation times, with one fixed at 2 ps, then the values of χ_R^2 are elevated 3–15-fold. Additionally, the values recovered for the amplitudes are not reasonable. Hence, the present data appear to exclude significant 2-ps motions of the tryptophan residues in either monomeric or tetrameric melittin.

DISCUSSION

Interpretation of the Melittin Anisotropy Decays

If these anisotropy decays are to be compared with molecular dynamic simulations, it is important that the data be interpreted properly. The parameter values (Θ_i and $r_0 g_i$) should be regarded as numerical descriptions of the decays, and should not be considered theoretically correct forms of the decay. As technology improves it is probable that higher resolution will be obtained, perhaps detecting motions intermediate between the fast and overall correlation times. Alternatively, further experimentation and analysis could reveal two longer correlation times that are the result of the axial ratio of the larger rotating unit. At present, the two correlation time fits seem to provide an adequate representation of the anisotropy decays of melittin monomer and tetramer.

The anisotropy decay for monomeric melittin is simple to interpret. The tryptophan residues are widely separated and the only process that can decrease the anisotropy is displacement of the tryptophan residue. In tetrameric melittin four tryptophan residues are located in a hydrophobic pocket. The distance between the two more closely spaced residues is 8 Å, and that between the more widely
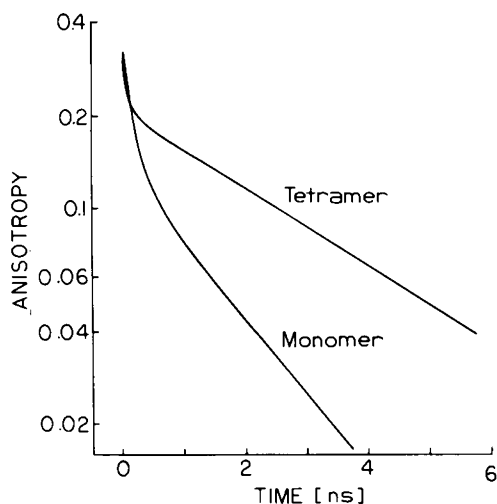
FIGURE 11 Anisotropy decays of melittin monomer and tetramer at 20°C from frequency-domain data with quenching. The anisotropy decay parameters for two correlation times from the simultaneous analysis (Tables VI and VII) were used to plot the time-dependent anisotropy decays. The parameters used are indicated by a double dagger.

spaced residues is 27 Å (Prendergast, F., personal communication). Using x-ray coordinates from D. Eisenberg (personal communication), we found similar distances. Since the Forster distance for indole-to-indole energy transfer is 14.8 Å in cyclohexane (37), we must consider the possible contribution of energy transfer to the anisotropy decay of the tetramer. However, we believe the Forster distance for tryptophan-to-tryptophan energy transfer in the tetramer is too small for significant energy transfer. From the absorption and emission spectrum of the tetramer, a quantum yield of 0.075 as compared with tryptophan (38), and a decay time of 2.5 ns, we calculated a Forster distance of 4.15 Å. This value is comparable to the experimental value of 6–7 Å for tryptophan-to-tryptophan transfer (39). These small Forster distances are the

TABLE VIII
ANISOTROPY DECAYS OF SYNTHETIC MELITTIN

[Acrylamide]	θ_i	$r_0 g_i$*	χ_R^2
M	ns		
No NaCl, monomer			
0, 0.2, and 0.5	0.28	0.149	
	1.79	0.107	1.2
	0.16	0.003	
	0.28	0.147	
	1.80	0.106	1.3
2 M NaCl, tetramer			
0, 0.2, and 0.5	0.08	0.072	
	3.62	0.210	1.0
	0.03	0.066	
	0.12	0.035	
	3.62	0.209	1.10

*The total anisotropy was a floating parameter.

result of the larger Stokes' shift and smaller spectral overlap of the absorption and emission spectra, relative to that of indole in cyclohexane. Two other experimental observations indicate that energy transfer among the tryptophans may not cause significant loss of anisotropy in the tetramer. Our excitation wavelength is on the red edge of the absorption (300 nm), and energy transfer among indole, tryptophanyl-tryptophan, polytryptophan, and many other fluorophores is known to fail on red edge excitation (40). Additionally, we previously observed that compression of the tetramer with hydrostatic pressure resulted in an increased anisotropy (41). If energy transfer depolarization was occurring the extent might be expected to increase as the tetramer volume was decreased. Hence we believe the 60-ps component in the tetramer anisotropy decay is due to torsional motions of the indole rings within the hydrophobic pocket of the tetramer. This rate and its associated amplitude should be compared with molecular dynamics simulation on this same protein. It may be necessary to examine an ensemble of melittin molecules to determine a sample-averaged anisotropy decay. The calculated decays should be compared with Fig. 11, which shows the anisotropy decays recovered from these experiments.

It is informative to interpret the anisotropy decays in terms of the angular displacement of the tryptophan residues. At any time the ratio of the anisotropy $(r(t))$ to the fundamental anisotropy (r_0) can be related to the average value of $\cos^2\Theta$ for an ensemble of protein molecules,

$$\frac{r(t)}{r_0} = \frac{3 < \cos^2\Theta > - 1}{2}. \tag{11}$$

Using this expression we can calculate the value of Θ after the rapid motions have exerted their effects. For the monomer and tetramer these values are 38° and 29°, respectively. It should be noted that $\Theta = 54.7$ in Eq. 11 is equivalent to complete depolarization. Alternatively, we can use the wobbling-in-a-cone model (9), for which Θ_c indicates the maximum angular displacement,

$$\frac{r(t)}{r_0} = [\frac{1}{2} \cos \Theta_c(1 + \cos \Theta_c)]^2. \tag{12}$$

For this model the anisotropy data indicate the tryptophan residues in the monomer and tetramer undergo local motions of 42° and 30°, respectively.

The qualitative features of our anisotropy decays are in agreement with those of Tran and Beddard (42). These workers also found shorter and longer correlation times, with the latter being those expected for overall rotations of the protein. The quantitative comparison is less satisfactory. Instead of short correlation times near 60–160 ps, Tran and Beddard obtained values of 500–700 ps. Additionally, these workers observed apparent r_0 values near 0.14, whereas the value expected for their 300-nm excitation is near 0.30. We suspect their data were not adequate to

766

recover the early portion of the anisotropy decay, resulting in the low apparent value of r_0 and the longer correlation time for the short component. This is the result expected for limited time-resolution, as shown by the simulations of Visser et al. (43).

Application to Time-Domain Fluorescence

Simultaneous analysis of progressively quenched samples should also provide increased resolution for time-domain measurements of anisotropy decays. Such a procedure would be analogous to the various "global" methods described by Brand and co-workers (44, 45). In time-domain fluorometry it is known that fast components in the anisotropy can decay within the lamp pulse, resulting in low apparent fundamental anisotropies (43). With conventional flash lamps, the pulses are 1–2-ns wide, and the lamp output is relatively weak (46). Hence, quenching may not be advantageous because the intensity will decay mostly within the lamp profile, and may become too weak for adequate measurements. However, these disadvantages should not be present with laser sources because their intensity is orders of magnitude greater than necessary for single photon counting, and the pulses from dye lasers are easily as short as 5 ps. Hence, simultaneous analysis of quenched emissions should also enhance the resolution obtained from time-domain anisotropy measurements.

REFERENCES

1. Weber, G. 1952. Polarization of the fluorescence of macromolecules. 1. Theory and Experimental Method. *Biochem. J.* 51:145–155.
2. Weber, G. 1952. Polarization of the fluorescence macromolecules. 2. Fluorescent conjugates of ovalbumin and bovine serum albumin. *Biochem. J.* 51:155–167.
3. Steiner, R. F. 1983. Excited States of Biopolymers. R. F. Steiner, editor. Plenum Publishing Corp., New York. 117–162.
4. Lakowicz, J. R. 1983. Principles of Fluorescence Spectroscopy. Plenum Publishing Corp., New York. 496 pp.
5. Belford, G. G., R. L. Belford, and G. Weber. 1972. Dynamics and fluorescence polarization and macromolecules. *Proc. Natl. Acad. Sci. USA.* 69:1392–1393.
6. Small, E. W., and I. Isenberg. 1977. Hydrodynamic properties of a rigid molecule: rotational and linear diffusion and fluorescence anisotropy. *Biopolymers.* 16:1907–1928.
7. Chuang, T. L., and K. B. Eisenthal. 1972. Theory of fluorescence depolarization by anisotropic rotational diffusion. *J. Chem. Phys.* 57:5094–5097.

8. Weber, G. 1977. Theory of differential phase fluorometry: detection of anisotropic molecular rotations. *J. Chem. Phys.* 66:4081–4091.
9. Kinosita, K., S. Kowata, and A. Ikegami. 1977. A theory of fluorescence polarization decay in membranes. *Biophys. J.* 20:289–305.
10. Lapari, G., and A. Szabo. 1980. Effect of librational motion on fluorescence depolarization and nuclear magnetic resonance relaxation in macromolecules and membranes. *Biophys. J.* 30:489–506.
11. Visser, A. J. W. G., and J. E. Wampler. 1985. Social symposium on time resolved fluorescence spectroscopy. *Anal. Instrum.* 14:193–561.
12. O'Connor, D. V., and D. Phillips. 1984. Time-Correlated Single Photon Counting. Academic Press, Inc., New York.
13. Demas, J. N. 1983. Excited State Lifetime Measurements. Academic Press, Inc., New York.
14. Magde, D., M. Zappala, W. H. Knox, and T. M. Nordlund. 1983. Picosecond fluorescence anisotropy decay in the ethidium/DNA complex. *J. Phys. Chem.* 87:3286–3288.
15. Nordlund, T. M., and D. A. Padolski. 1983. Streak camera measurements of tryptophan and rhodamine motions with picosecond time resolution. *Photochem. Photobiol.* 38:665–669.
16. Gratton, E., and M. Limkeman. 1983. A continuously variable frequency cross-correlation phase fluorometer with picosecond resolution. *Biophys. J.* 44:315–324.
17. Lakowicz, J. R., and B. P. Maliwal. 1985. Construction a performance of a variable-frequency phase-modulation fluorometer. *Biophys. Chem.* 21:61–78.
18. Lakowicz, J. R., G. Laczko, and I. Gryczynski. 1986. A 2 GHz frequency-domain fluorometer. *Rev. Sci. Instrum.* 57:2499–2506.
19. Lakowicz, J. R., G. Laczko, and I. Gryczynski. 1987. Picosecond resolution of tyrosine fluorescence and anisotropy decays by 2 GHz frequency-domain fluorometry. *Biochemistry.* 26:82–90.
20. Lakowicz, J. R., H. Cherek, B. P. Maliwal, and E. Gratton. 1985. Time-resolved fluorescence anisotropies of fluorophores in solvents and lipid bilayers obtained from frequency-domain phase-modulation fluorometry. *Biochemistry.* 24:376–383.
21. Maliwal, B. P., and J. R. Lakowicz. 1986. Resolution of complex anisotropy decays by variable frequency phase-modulation fluorometry: a simulation study. *Biochim. Biophys. Acta.* 873:161–172.
22. Lakowicz, J. R., G. Laczko, I. Gryczynski, and H. Cherek. 1986. Measurement of subnanosecond anisotropy decays of protein fluorescence using frequency-domain fluorometry. *J. Biol. Chem.* 261:2240–2245.
23. Lakowicz, J. R., E. Gratton, G. Laczko, H. Cherek, and M. Limkeman. 1984. Analysis of fluorescence decay kinetics from variable-frequency phase shift and modulation data. *Biophys. J.* 46:463–477.
24. Talbot, J. C., J. Dufourcq, J. deBong, J. R. Faucon, and C. Lurson. 1979. Conformational change and self-association of monomeric melittin. *FEBS (Fed. Eur. Biochem. Soc.) Lett.* 102:191–193.
25. Eftink, M. R., and C. A. Ghiron. 1976. Fluorescence quenching of indole and model micelle systems. *J. Phys. Chem.* 80:486–493.
26. Lakowicz, J. R. 1987. Modern Physical Methods. L. M. van Deenen, editor. Elsevier Biomedical Press, Amsterdam. In press.
27. Lakowicz, J. R., M. L. Johnson, N. Joshi, and I. Gryzcynski. 1987. Transient effects in quenching detected by harmonic-content frequency-domain fluorometry. *J. Phys. Chem.* In press.
28. Nemzek, T. L., and W. R. Ware. 1975. Kinetics of diffusion-controlled reactions: transient effects in fluorescence quenching. *J. Chem. Phys.* 62:477–489.
29. Bevington, P. R. 1969. Data Reduction and Error Analysis for the Physical Sciences. McGraw-Hill, Inc., New York. 336 pp.
30. Karplus M., and J. A. McCammon. 1981. The internal dynamics of globular proteins. *CRC Crit. Rev. Biochem.* 9:293–349.
31. van Gunsteren, W. F., and M. Karplus. 1982. Protein dynamics in

solution and in a crystalline environment: a molecular dynamics study. *Biochemistry.* 21:2259–2274.

32. Karplus, M., B. R. Gelin, and J. A. McCammon. 1980. Internal dynamics of proteins: short time and long time motions of aromatic side chains in PTI. *Biophys. J.* 32:603–618.

33. Levy, R. M., and A. Szabo. 1982. Initial fluorescence depolarization of tyrosines in proteins. *J. Am. Chem. Soc.* 104:2073–2075.

34. Ichiye, T., and M. Karplus. 1983. Fluorescence depolarization of tryptophan residues in proteins: a molecular dynamics study. *Biochemistry.* 22:2884–2893.

35. Faucon, J. F., J. Dufourcq, and C. Lurson. 1979. The self-association of melittin and its binding to lipids. *FEBS (Fed. Eur. Biochem. Soc.) Lett.* 102:187–190.

36. Terwilliger, T. C., and D. Eisenberg. 1982. The structure of melittin, II. Interpretation of the structure. *J. Biol. Chem.* 257:6016–6022.

37. Berlman, I. B. 1973. Energy Transfer Parameters of Aromatic Compounds. Academic Press, Inc., New York. 253–254.

38. Chen, R. F. 1967. Fluorescence quantum yields of Tryptophan and Tyrosine. *Anal. Lett.* 1:35–42.

39. Steinberg, I. Z. 1971. Long-range nonradiative transfer of electronic excitation energy in patients and polypeptides. *Annu. Rev. Biochem.* 40:83–114.

40. Weber, G., and M. Shinitzky. 1970. Failure of energy transfer between identical aromatic molecules on excitation at the long wavelength edge of the absorption spectrum. *Proc. Natl. Acad. Sci. USA.* 65:823–830.

41. Thompson, R. B., and J. R. Lakowicz. 1984. Effect of pressure on the self-association of melittin. *Biochemistry.* 23:3411–3417.

42. Tran, C. D., and G. S. Beddard. 1985. Studies of the fluorescence from tryptophan in melittin. *Eur. J. Biochem.* 13:59–64.

43. Visser, A. J. W. J., T. Ykema, A. van Hoek, D. J. O'Kane, and J. Lee. 1985. Determination of rotational correlation times from deconvoluted fluorescence anisotropy decay curves. Demonstration with 6,7-dimethyl-8-ribityllumazine and lumazine protein from photobacterium leiognathi as fluorescent indicators. *Biochemistry.* 24:1489–1496.

44. Beechem, J. M., J. R. Knutson, J. A. B. Ross, B. J. Turner, and L. Brand. 1983. Global resolution of heterogeneous decays by phase/modulation fluorometry. *Biochemistry.* 22:6054–6058.

45. Knutson, J. R., J. M. Beechem, and L. Brand. 1983. Simultaneous analysis of multiple fluorescence decay curves: a global approach. *Chem. Phys. Lett.* 1-2:501–507.

46. Lakowicz, J. R. 1986. A review of photon counting and phase-modulation measurements of fluorescence decay kinetics. *In* Applications of Fluorescence in the Biomedical Sciences. D. L. Taylor, A. S. Waggoner, R. F. Murphy, F. Lanni, and R. R. Birge, editors. Alan R. Liss, Inc., New York. 29–67.